

Gas/Particle Partitioning and Secondary Organic Aerosol Yields

JAY R. ODUM,[†]
 THORSTEN HOFFMANN,[‡]
 FRANK BOWMAN,[§] DON COLLINS,[†]
 RICHARD C. FLAGAN,[§] AND
 JOHN H. SEINFELD^{*,§}

*Department of Environmental Engineering Science and
 Department of Chemical Engineering, California Institute of
 Technology, Pasadena, California 91125*

Secondary organic aerosol (SOA) formation is considered in the framework of the gas/particle partitioning absorption model outlined by Pankow (1, 2). Expressions for the fractional SOA yield (Y) are developed within this framework and shown to be a function of the organic aerosol mass concentration, M_o . These expressions are applied to over 30 individual reactive organic gas (ROG) photooxidation smog chamber experiments. Analysis of the data from these experiments clearly shows that Y is a strong function of M_o and that secondary organic aerosol formation is best described by a gas/particle partitioning absorption model. In addition to the 30 individual ROG experiments, three experiments were performed with ROG mixtures. The expressions developed for Y in terms of M_o , used in conjunction with the overall yield data from the individual ROG experiments, are able to account for the M_o generated in the ROG mixture experiments. This observation not only suggests that SOA yields for individual ROG are additive but that smog chamber SOA yield data may be confidently extrapolated to the atmosphere in order to determine the important ambient sources of SOA in the environment.

Introduction

It is now well recognized that secondary organic matter can significantly contribute to the particulate burden in urban atmospheres. However, because of the enormous complexity of the chemical matrix of organic aerosol and the lack of direct chemical analysis methods for a majority of the compounds comprising the organic aerosol fraction, estimates of secondary organic aerosol (SOA) contributions in the urban environment have been restricted to indirect

methods of determination. For example, Turpin and Huntzicker used correlations between measured organic carbon (OC) and elemental carbon (EC) to estimate SOA contributions in Los Angeles during the summer Southern California Air Quality Study (SCAQS) in 1987 (3). The study showed that as much as 70% of the organic aerosol can be of secondary origin under peak photochemical conditions. Other estimates, based on chemical mass balance methods, suggest that on a yearly average, 20–30% of the fine organic particulate matter in the South Coast Air Basin may be secondary (4).

Efforts to represent SOA formation in ambient models have primarily been based on using experimentally determined fractional aerosol yields (5–7). The fractional aerosol yield (Y), defined as the fraction of a reactive organic gas (ROG) that is converted to aerosol, is calculated by

$$Y = \frac{\Delta M_o}{\Delta \text{ROG}} \quad (1)$$

where ΔM_o is the organic aerosol mass concentration ($\mu\text{g m}^{-3}$) produced for a given amount of ROG reacted, ΔROG ($\mu\text{g m}^{-3}$). Aerosol yields have been estimated from smog chamber data for a variety of ROG by various researchers over the last 20 years (8–15). In general, measured yields for a single compound have shown a wide degree of variation both between and within laboratories. For example, observed SOA yields for α -pinene range from less than 10% to greater than 50% (5, 16). Several factors likely contribute to this dramatic variability, but the major factor may be the way that SOA formation has been represented.

Secondary aerosols are formed by reaction of an ROG to produce both semivolatile and nonvolatile products. Previously, it has been assumed that the vapor-phase products begin to condense onto existing seed particles (or to homogeneously nucleate) only after a product exceeds its saturation concentration and that the amount of a product that condenses is the quantity in excess of its saturation concentration. For the initial condensation process and certainly for the initial nucleation process, this may be the case. However, Pankow has suggested that, once organics have begun to condense and an organic layer has formed on the particles, even products whose gas-phase concentrations are below their saturation concentrations will partition a portion of their mass into this condensed organic phase (2). For each compound that partitions into the absorbing organic material (om) phase, Pankow has defined an absorption equilibrium constant ($K_{p,i}$) as

$$K_{p,i} = \frac{F_{i,om}}{A_i \text{TSP}} = \frac{760RTf_{om}}{\text{MW}_{om} 10^6 \zeta_i p_{L,i}^\circ} \quad (2)$$

where A_i is the gas phase concentration (ng m^{-3}) of compound i , $F_{i,om}$ is the concentration of compound i (ng m^{-3}) in the absorbing om phase, TSP is the total suspended particulate concentration ($\mu\text{g m}^{-3}$), R is the ideal gas constant ($8.206 \times 10^{-5} \text{ m}^3 \text{ atm mol}^{-1} \text{ K}^{-1}$), T is temperature (K), f_{om} is the mass fraction of the TSP that is the absorbing om phase, MW_{om} is the mean molecular weight of the absorbing om (g mol^{-1}), ζ_i is the activity coefficient of compound i in the om phase, and $p_{L,i}^\circ$ is the vapor pressure

* To whom correspondence should be addressed; e-mail address: april@macpost.caltech.edu.

[†] Department of Environmental Engineering Science.

[‡] Present address: Institute für Spektrochemie und Angewandte Spektroskopie D-44139, Dortmund, Germany.

[§] Department of Chemical Engineering.

(Torr) of the absorbing compound as a liquid (subcooled, if necessary).

Considering only the mass of the om phase, one can similarly define a partitioning coefficient for species i ($K_{om,i}$) in terms of the organic mass concentration

$$K_{om,i} = \frac{F_{i,om}}{A_i M_o} = K_{p,i} / f_{om} \quad (3)$$

where like K_p , K_{om} has units of ($\text{m}^3 \mu\text{g}^{-1}$), and M_o is the absorbing organic mass concentration ($\mu\text{g m}^{-3}$). This equilibrium partitioning coefficient suggests that, for $K_{om,i}$ to be constant for a given compound, the fraction of a compound's total mass residing in the particulate phase will increase with increasing organic mass concentrations. This behavior for the semivolatile products involved in SOA formation would lead to the high variability found for published values of SOA yields for a given ROG, since the fractional aerosol yields will be dependent on the organic aerosol mass concentration.

Pandis et al. state that two of the three major uncertainties in predictions of ambient SOA are the discrepancies in experimentally determined SOA yields and in the partitioning of the condensable vapors between the gas and aerosol phases (6). In this paper, both of these factors will be addressed. We shall use the partitioning theory of Pankow (1, 2) to develop expressions for the fractional secondary aerosol yield (Y) in terms of organic mass concentration. These expressions are then applied to over 30 SOA smog chamber experiments conducted in the summer of 1995. This analysis is used to show how SOA smog chamber data can be used to identify the important sources of SOA in the urban environment.

Experimental Description

Experiments were performed in a 60- m^3 sealed collapsible Teflon bag that has been described in detail previously (8, 9). Most of these experiments were conducted in a dual-chamber mode, in which the bag was divided in the center with a clamped PVC pipe, so that two different experiments could be conducted under identical environmental (i.e., sunlight intensity, temperature, etc.) conditions. The two resulting chambers had volumes of approximately 20 m^3 . The gas-phase instrumentation and aerosol data acquisition system are housed in a laboratory adjacent to the chamber. All aerosol sampling equipment was housed in a cart adjacent to the chamber that was maintained at a constant temperature of 25 °C. Prior to every experiment, the chamber was continuously flushed with purified laboratory compressed air for at least 38 h and baked in sunlight for at least 1 day. The compressed air was processed through three consecutive packed-bed scrubbers containing, in order, Purafil, Drierite and 13 \times molecular sieves, and activated charcoal. After purification, the air was rehumidified to a relative humidity of approximately 10% with distilled/dionized water before entering the chamber. The resulting air contained no detectable reactive hydrocarbons, no particles, and less than 5 ppb NO_x .

Hydrocarbon measurements were made using a Hewlett Packard (Palo Alto, CA) 5890 gas chromatograph (GC) that was equipped with a DB-5 column (J&W Scientific, Davis, CA) and a flame ionization detector (FID). The GC temperature program was as follows: -60 °C for 1 min, -60 to 100 °C at 40 °C min^{-1} , and hold at 100 °C for 1 min. Hydrocarbon calibrations were performed prior to each

experiment either using certified gas mixtures or by vaporizing microliter volumes of a calibration solution of the pure hydrocarbon in CH_2Cl_2 into a 60-L Teflon bag filled with a measured volume of Ultra Zero (Air Liquid America Corp., Houston, TX) compressed air.

The calibrations were generally followed by injection of $(\text{NH}_4)_2\text{SO}_4$ seed particles to obtain particle concentrations of 5000–10 000 particles cm^{-3} with a number mean diameter of approximately 100 nm. The particles were generated by atomizing an aqueous solution of $(\text{NH}_4)_2\text{SO}_4$ using a stainless steel, constant rate atomizer. The aerosol was passed through heated copper tubing into a diffusional dryer, followed by a ^{85}Kr charge neutralizer before entering the chamber.

After obtaining the desired initial seed particle concentration, propene, hydrocarbons, NO_x , and hexafluorobenzene (C_6F_6) were injected (approximately 1 h prior to the start of the experiment) through Teflon lines into the chamber, which was completely shrouded from sunlight with a black polyethylene tarpaulin. Propene, NO, and NO_2 were injected using certified cylinders containing approximately 500 ppm of the gas in nitrogen. Hydrocarbons and C_6F_6 were introduced into the chamber by injecting microliter quantities of the pure liquid compound into a glass bulb that was gently heated while being diluted with purified compressed lab air that went directly to the chamber. Propene was used at mixing ratios of 250–350 ppb to generate OH radicals in sufficient concentrations for the inception of the experiment. C_6F_6 was used as an internal standard for hydrocarbon gas chromatographic (GC) samples in order to normalize for injection variations of the six-port stainless steel injection valve (Valco, Houston, TX), equipped with a heated (100 °C) 2-mL Teflon sampling loop. The half-life of C_6F_6 in the chamber was of the order of several days ($k_{\text{OH}} = 1.72 \times 10^{-13} \text{ cm}^3 \text{ molecule}^{-1} \text{ s}^{-1}$), and so its concentrations were stable for times much longer than the typical experiment, allowing it to serve as an excellent internal standard. The use of the internal standard yielded estimated uncertainties in the hydrocarbon measurements of less than $\pm 2\%$ for most experiments.

After injection of the gases and seed aerosol, but before uncovering the chamber, initial measurements of hydrocarbons, NO_x , O_3 , and aerosol concentrations and size distributions were made to obtain initial values and to ensure that the contents were well mixed. Generally, three to five initial hydrocarbon measurements, using the HP 5890 GC described above, were made for each side of the bag. A Thermo Environmental Instruments (Franklin, MA) Model 42 chemiluminescence NO_x monitor was used to measure NO, NO_2 , and NO_x . Prior to the start of each experiment, a zero/span calibration was performed on the NO_x monitor using certified cylinders of NO and NO_2 . In addition, a complete calibration of the NO_x monitor was performed on approximately a weekly basis. A Dasibi Environmental Corp. (Glendale, CA) Model 1008-PC O_3 analyzer was used to monitor O_3 concentrations. The NO_x and O_3 measurements were made at 10-min intervals between alternating sides of the chamber. The estimated uncertainties in the NO and NO_2 measurements are approximately $\pm 4\%$ and $\pm 7\%$, respectively. The ozone instrument has an estimated uncertainty of $\pm 4\%$ in its initial calibration and was seen to drift only a few percent over the period of several months.

Complete number and size distribution measurements were recorded for both sides of the chamber with a 1-min

frequency throughout an experiment. The aerosol instrumentation consisted of one radial scanning electrical mobility spectrometer (17) and one TSI Model 3071 cylindrical scanning electrical mobility spectrometer for each side of the divided chamber. All four scanning electrical mobility spectrometers (SEMS) were equipped with either a model 3760 or model 3025 TSI condensation nuclei counter (CNC) to count transmitted particles. SEMS voltages were scanned from 40 to 8500V with a 1-min ramp. The radial SEMS were operated with sheath and excess flows of 15 L min⁻¹ and inlet and classified aerosol flows of 1.5 L min⁻¹ to allow for measurement of particle size distributions over the range of 5–80 nm. The cylindrical SEMS were operated with sheath and excess flows of 2.5 L min⁻¹ and inlet and classified aerosol flows of 0.25 L min⁻¹ to allow for measurement of particle size distributions in the range of 30–850 nm. A more complete description of the SEMS scanning cycle and operation has been published previously (9). Particle losses in the SEMS, SEMS response functions, particle charging efficiencies, CNC counting efficiency, and particle deposition in the chamber have been taken into account in the analysis of the aerosol data (9). The estimated uncertainty in the SEMS size and concentration measurements are approximately $\pm 10\%$.

After making initial measurements prior to the start of the experiment, the black tarpaulin (chamber cover) was removed to begin the photooxidation experiment. Hydrocarbon measurements were made for both sides of the chamber every 8–10 min throughout the experiment. NO, NO₂, NO_x, and O₃, were continuously monitored during 10-min intervals alternating between the two sides of the chamber. Temperature, total solar radiation, and UV were continuously monitored over the course of the experiment.

Results and Discussion

Expressions for SOA Yields. In the presence of absorption partitioning of secondary organic aerosol species, fractional aerosol yields should be dependent on the total organic aerosol mass concentration. In order to derive the functional form of this dependence, let us begin by assuming that the concentrations of the dozens of individual products that result from the photooxidation of an ROG are proportional to the amount of ROG that reacts (ΔROG) such that

$$1000\alpha_i \Delta\text{ROG} = C_i \quad (4)$$

where α_i is the proportionality constant relating the concentration of ROG that reacts to the total concentration of product i (C_i) that is formed. The total concentration of a product that is formed is simply the concentration of the product that is in the gas phase (A_i) plus the concentration of the product that is in the aerosol phase (F_i). The factor of 1000 in eq 4 is needed because the units of ΔROG are $\mu\text{g m}^{-3}$ and the units of C_i are ng m^{-3} . Since the parent ROG and the products have different molecular weights, α_i is actually the product of the stoichiometric factor for the reaction forming product i and the ratio of the molecular weight of product i to the molecular weight of the parent ROG.

The desired property of the aerosol yield (Y) is that it possess a value that, when multiplied by the total mass of an ROG that reacts, gives the total mass of products that

end up in the aerosol phase

$$Y(1000V_c\Delta\text{ROG}) = \sum_i (F_i V_c) \quad (5)$$

where V_c is the volume in which the reaction takes place, and once again a factor of 1000 is needed due to the difference in units for ΔROG and F_i . Combining eqs 3–5 and using the mass balance constraint (i.e., $C_i = A_i + F_i$) gives the following expression for the yield of an individual product (Y_i):

$$Y_i = M_o \left(\frac{\alpha_i K_{om,i}}{1 + K_{om,i} M_o} \right) \quad (6)$$

Similarly, the expression for the overall SOA yield (Y) is given by

$$Y = \sum_i Y_i = M_o \sum_i \left(\frac{\alpha_i K_{om,i}}{1 + K_{om,i} M_o} \right) \quad (7)$$

Equations 6 and 7 have several interesting features. First, they suggest that for low organic mass concentrations and for products that have relatively small partitioning coefficients, the SOA yield will be directly proportional to the total aerosol organic mass concentration, M_o . Secondly, for very nonvolatile products and/or for large organic mass concentrations, the individual product yields will be independent of the organic mass concentration and will be equal to α_i . Finally, they suggest that the individual yields for the more volatile products will be sensitive to temperature since $K_{om,i}$ is inversely proportional to the vapor pressure of the species (see eqs 2 and 3). If the semivolatile products involved in SOA formation exhibit the type of partitioning behavior indicated in eqs 6 and 7, then it is highly unlikely that a particular ROG will have a unique fractional aerosol yield. Instead, it will exhibit a range of yields over a range of organic mass concentrations.

Experimentally Determined SOA Yields. A list of the SOA experiments that are discussed in this paper are summarized in Table 1. Over 30 experiments were performed with *m*-xylene, 1,2,4-trimethylbenzene, and α -pinene. Table 1 lists the date on which the experiment was performed, the initial ROG concentrations (ROG_0), the total amount of ROG consumed in each experiment (ΔROG), the total organic aerosol mass that was produced (M_o), the initial NO_x concentration, the initial propene concentration (C_3H_6), the ratio of consumed hydrocarbon to initial NO_x ($\Delta\text{HC}/\text{NO}_x$), and the overall SOA yield (Y). Total organic aerosol mass concentration was calculated from the observed total organic aerosol volume, assuming a density of 1 g cm^{-3} .

SOA Yields of Aromatics. The functional form of eq 7 suggests that fractional aerosol yields should be a function of organic aerosol mass concentrations. For example, fractional aerosol yields (Y) versus organic aerosol mass concentrations (M_o) for *m*-xylene and 1,2,4-trimethylbenzene are shown in Figures 1 and 2. As is evident from the figures, Y is a strong function of the value of M_o . It can be seen that for small M_o , the yield increases rapidly with increasing M_o and becomes a weaker function of M_o at higher concentrations, in accord with the behavior predicted by eq 7. The lines through the data in Figures 1 and 2 have been generated from eq 7 assuming that there are two products that partition to the absorbing om phase to a measurable degree for each ROG. Values for α_1 , α_2 , $K_{om,1}$, and $K_{om,2}$ are chosen to fit the data for each ROG by

TABLE 1

Outdoor Smog Chamber Experiment Summary

	date	ROG ₀ (μg m ⁻³)	ΔROG (μg m ⁻³)	M ₀ (μg m ⁻³)	NO _x (ppb)	C ₃ H ₆ (ppb)	ΔHC/NO _x (ppb of C/ppb)	Y (%)
<i>m</i> -xylene	07/27A	2264	2114	101	629	300	7.8	4.78
<i>m</i> -xylene	07/27B	399	362	1.7	342	300	4.6	0.47
<i>m</i> -xylene	07/31A	1423	1219	20.1	521	235	6.0	1.64
<i>m</i> -xylene	07/31B	1494	1290	38.1	528	245	6.1	2.95
<i>m</i> -xylene	08/04A	4194	3953	396	1697	300	4.9	10.0
<i>m</i> -xylene	08/04B	2160	2018	106	933	300	4.9	5.25
<i>m</i> -xylene	08/09B	1049	795	18.8	1077	325	2.4	2.36
<i>m</i> -xylene	08/11A	1136	728	26.5	130	265	16.9	3.64
<i>m</i> -xylene	08/11B	1203	945	23.0	235	263	11.1	2.43
<i>m</i> -xylene	09/11A	1215	861	32.0	146	421	20.2	3.72
<i>m</i> -xylene	09/11B	1248	1032	35.5	279	421	11.8	3.44
<i>m</i> -xylene	09/13A	1211	1028	21.4	231	294	12.4	2.08
<i>m</i> -xylene	09/13B	1252	774	1.5	1609	294	1.3	0.19
<i>m</i> -xylene + α-pinene	09/15A	1394 + 278	1207 + 278	80.3	503	300	7.4	
<i>m</i> -xylene + α-pinene	09/19A	1132 + 342	936 + 342	82.2	409	300	8.1	
<i>m</i> -xylene	10/17A	2331	1945	188	998	300	4.5	9.67
1,2,4-Tmb	10/17B	2391	1996	113	975	300	4.7	5.66
1,2,4-Tmb	11/02A	3367	2282	155	1178	300	4.3	6.79
1,2,4-Tmb	11/02B	1607	1198	43.0	490	300	6.3	3.59
1,2,4-Tmb	11/07A	1932	1533	78.0	590	300	6.3	5.09
1,2,4-Tmb	11/07B	1237	1020	26.5	359	300	7.7	2.60
1,2,4-Tmb	11/09B	1745	1309	53.0	528	300	6.2	4.05
1,2,4-Tmb + <i>m</i> -xylene	11/09A	1633 + 1538	1270 + 979	195	1048	300	4.8	
α-pinene	08/14A	726	726	87.0	240	300	9.8	12.0
α-pinene	08/14B	769	769	96.0	240	300	10.2	12.5
α-pinene	08/17A	384	384	22.7	203	300	8.0	5.91
α-pinene	08/17B	104	104	1.3	113	300	9.7	1.25
α-pinene	09/15B	283	283	8.0	206	300	6.9	2.83
α-pinene	09/22A	505	505	33.0	135	300	13.7	6.53
α-pinene	09/22B	467	467	38.2	125	300	14.5	8.18
α-pinene	09/25A	510	510	39.3	124	300	14.9	7.71
α-pinene	09/25B	505	505	34.2	122	300	15.1	6.77

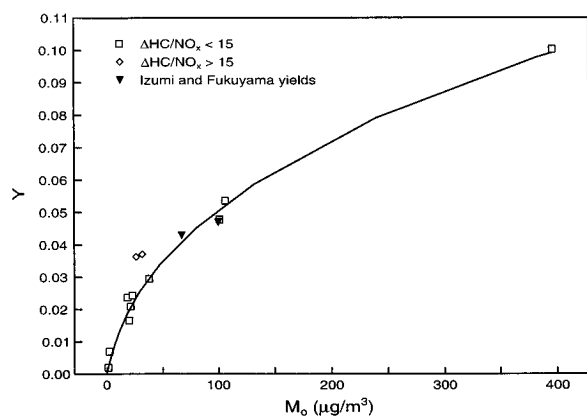


FIGURE 1. SOA yields for *m*-xylene as a function of M_0 . Values used to generate the two-product model line are 0.03, 0.167, 0.032, and 0.0019 for α_1 , α_2 , $K_{om,1}$, and $K_{om,2}$, respectively.

minimizing the square of the residuals. Two products are the minimum number needed to fit the behavior of the system. A one-product model is insufficient to represent the shape of the curve, and three or more products are superfluous. Since it is known that there are dozens of products in the particle phase from the reactions of these two aromatics, the four constants that were chosen to fit the data for each ROG have no actual physical meaning, other than perhaps as an average of all the α and K_{om} values. However, the degree of fit to the data does suggest that the functional form of eq 7 captures the dependence of Y on M_0 and that fractional aerosol yields do indeed depend on organic aerosol mass concentrations. This dependence also offers an explanation for observed increasing yields for increasing amounts of ROG reacted (8, 16); as more ROG

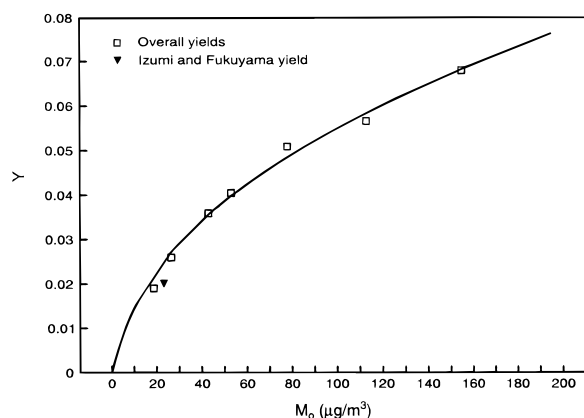


FIGURE 2. SOA yields for 1,2,4-trimethylbenzene as a function of M_0 . Values used to generate the two-product model line are 0.0324, 0.166, 0.053, and 0.002 for α_1 , α_2 , $K_{om,1}$, and $K_{om,2}$, respectively.

reacts, more condensed organic mass is produced, leading to a higher observed yield.

The data points in Figure 1 come from data obtained from 12 experiments that cover a range of initial hydrocarbon concentrations from 399 to 4194 $\mu\text{g m}^{-3}$ (96–1008 ppb) and a range of $\Delta\text{HC}/\text{NO}_x$ ratios from 1.3 to 20.2 ppb of C/ppb (Table 1). The model line through the data was chosen to fit the data points that were obtained from the experiments with $\Delta\text{HC}/\text{NO}_x$ ratios less than 15. As can be seen in the figure, the two points with a $\Delta\text{HC}/\text{NO}_x$ ratio greater than 15 have yields that are slightly higher than those with ratios less than 15. So it appears that the fractional aerosol yield for *m*-xylene is slightly dependent upon $\Delta\text{HC}/\text{NO}_x$. This is not surprising considering that

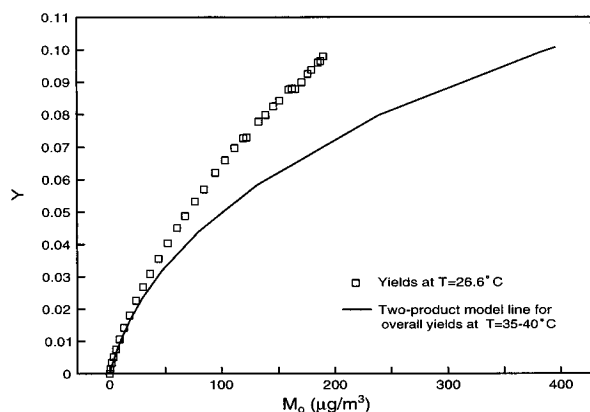


FIGURE 3. Comparison of temperature dependence of *m*-xylene SOA yields. Two-product model line is from data in Figure 1, which corresponds to experiments conducted at 35–40 °C. Data points correspond to yields for experiment 10/17A, which was conducted at 26.6 ± 1 °C.

the photooxidation product distributions will depend on $\Delta\text{HC}/\text{NO}_x$. However, the data suggest that the effect on the yield is minimal.

The yields in Figure 1 and 2 were calculated using eq 1, where ΔM_0 is the total organic aerosol mass concentration that was produced and ΔROG is the total amount of ROG that reacted over the course of an experiment. Most of the data in Figures 1 and 2 are from the experiments that were conducted in our laboratory in the summer and fall of 1995 (Table 1). However, two of the data in Figure 1 and one datum in Figure 2 are those of Izumi and Fukuyama (11). The points from the data of Izumi and Fukuyama agree quite well with the Caltech measurements and further demonstrate the generality of the dependence of Y on M_0 .

The temperature dependence of Y is illustrated in Figure 3. The line in the figure is the two-product model line used to fit the data in Figure 1, which corresponds to experiments that were conducted in the temperature range of 35–40 °C. The data points in Figure 3 correspond to yield data that were obtained from an experiment (10/17A) that was conducted at 26.6 ± 1 °C. As eqs 2 and 7 suggest, Y seems to be a strong function of temperature. Since K_{om} is inversely proportional to the pure component vapor pressure, the yield is higher at lower temperatures for a given M_0 . The yield values from Izumi and Fukuyama (11) agree better with the higher temperature yields from this group even though they were generated at a temperature closer to the lower temperature run from this group. The most likely cause for this discrepancy is that Izumi and Fukuyama (11) did not take aerosol deposition losses into account in estimating their yields and, therefore, probably slightly underestimated the yield values for the temperature at which they were obtained. However, it is still remarkable that the values obtained by Izumi and Fukuyama agree so well with the Caltech data when viewed in terms of organic aerosol mass concentrations.

The SOA yields for 1,2,4-trimethylbenzene that are shown in Figure 2 are from experiments that were conducted at temperatures from 22 to 26 °C. The yield values are very similar to those for both the lower and higher temperature *m*-xylene data at organic mass concentrations below $60 \mu\text{g m}^{-3}$. At organic mass concentrations above $60 \mu\text{g m}^{-3}$, the yields for 1,2,4-trimethylbenzene are higher than those for the higher temperature *m*-xylene data and lower than those for the lower temperature *m*-xylene data. Thus, for most atmospherically relevant M_0 values (i.e., $60 \mu\text{g m}^{-3}$ or less),

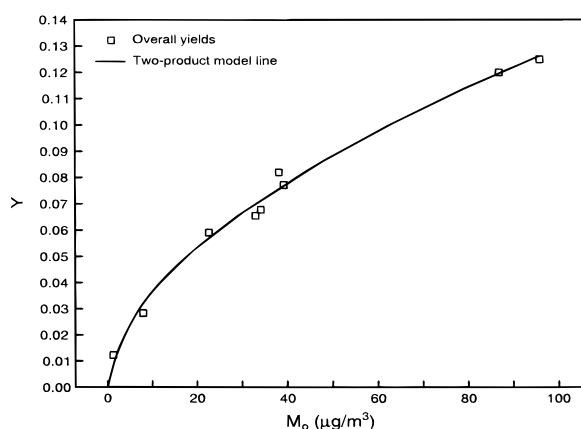


FIGURE 4. SOA yields for α -pinene as a function of M_0 . Values used to generate the two-product model line are 0.038, 0.326, 0.171, and 0.004 for α_1 , α_2 , $K_{om,1}$, and $K_{om,2}$, respectively.

1,2,4-trimethylbenzene has a similar yield to *m*-xylene for a given organic mass concentration. This is not all that surprising considering that the types of products that are formed from the oxidation of these two aromatic species are quite similar.

SOA Yields of α -Pinene. SOA smog chamber experiments were also conducted with α -pinene. The overall yields (Y) for α -pinene versus M_0 are shown in Figure 4. As for *m*-xylene and trimethylbenzene, the line through the data is generated using a two-product model, where α_1 , α_2 , $K_{om,1}$, and $K_{om,2}$ were chosen to fit the data by minimizing the square of the residuals. Yields for α -pinene follow the same trend with M_0 as do those for the aromatics but are considerably higher for a given M_0 . For example, the yield for α -pinene at an M_0 of $50 \mu\text{g m}^{-3}$ is 8.85% while that for *m*-xylene is 3.3%. As with the majority of the experiments for *m*-xylene, the experiments for α -pinene were conducted at 35–40 °C. The yields are expected to be even higher for lower temperatures. Also the yield experiments for α -pinene were conducted over a range of $\Delta\text{HC}/\text{NO}_x$ ratios of 6.9–15.1. There was little observed dependence of the yield on the ratio.

SOA Yields for ROG Mixtures. In addition to the individual ROG experiments, three multiple ROG experiments were also conducted. Two experiments were performed with a mixture of *m*-xylene and α -pinene, and one experiment was conducted with a mixture of *m*-xylene and 1,2,4-trimethylbenzene. These experiments were used to further test the hypothesis that Y is a function of organic aerosol mass concentrations. In both cases, selected concentrations of the two ROGs were placed in the chamber together with NO_x and irradiated with sunlight. The initial ROG concentrations, $\Delta\text{HC}/\text{NO}_x$ ratios, and the final M_0 values are listed in Table 1. The two experiments with *m*-xylene and α -pinene were conducted at temperatures between 35 and 40 °C.

In experiment 09/15A, a maximum organic aerosol mass concentration of $80.3 \mu\text{g m}^{-3}$ was generated by the end of the experiment. Using the model generated lines in Figures 1 and 4, an M_0 of $80.3 \mu\text{g m}^{-3}$ corresponds to a yield of 4.4% for *m*-xylene and a yield of 11.5% for α -pinene. Multiplying the value for *m*-xylene by the amount of *m*-xylene that reacted ($1207 \mu\text{g m}^{-3}$) gives an M_0 of $53.1 \mu\text{g m}^{-3}$. Multiplying the value for α -pinene by its amount reacted ($278 \mu\text{g m}^{-3}$) gives an M_0 of $32.0 \mu\text{g m}^{-3}$. The sum of these two values is $85.1 \mu\text{g m}^{-3}$, which is extremely close to the overall observed organic aerosol mass concentration of 80.3

$\mu\text{g m}^{-3}$ that was generated from the mixture of the two ROG. This observation lends strong support to the idea that eq 7 correctly describes the dependence of SOA yields on organic aerosol mass concentrations.

A second multiple ROG experiment (09/19A) was conducted with *m*-xylene and α -pinene, and the final M_0 that was generated from the combined oxidation of these two ROG was $82.2 \mu\text{g m}^{-3}$. If one goes through the same procedure as above, using Figures 1 and 4 to obtain the appropriate yield values that correspond to an M_0 of $82.2 \mu\text{g m}^{-3}$, the combined single M_0 values add up to $81.2 \mu\text{g m}^{-3}$. Once again the yields for the individual hydrocarbons, when used in conjunction with eq 7, are capable of accounting for the total organic aerosol mass concentrations that are produced from the oxidation of the ROG mixture.

A multiple ROG experiment with *m*-xylene and 1,2,4-trimethylbenzene was also conducted. The experiment was performed at a temperature of $25.5 \pm 2^\circ\text{C}$, and the final organic aerosol mass concentration was $195 \mu\text{g m}^{-3}$. Since the experiment was conducted at $25.5 \pm 2^\circ\text{C}$, the two product model line for *m*-xylene in Figure 1 that applies at $35\text{--}40^\circ\text{C}$ cannot be used. However the data points for experiment 10/17A in Figure 3 were obtained at $26.6 \pm 1^\circ\text{C}$. Using these points to generate a two-product model line gives a yield of 9.94% for *m*-xylene at an M_0 of $195 \mu\text{g m}^{-3}$ and a temperature of 26.6°C . Using the model line for 1,2,4-trimethylbenzene in Figure 2, the yield is 7.61% at an M_0 of $195 \mu\text{g m}^{-3}$. Multiplying these yields for each of the ROG by the amount that each ROG reacted gives M_0 values of $97.3 \mu\text{g m}^{-3}$ for *m*-xylene and $97.6 \mu\text{g m}^{-3}$ for 1,2,4-trimethylbenzene. The sum of these is $194.9 \mu\text{g m}^{-3}$, which is virtually identical to the M_0 of $195 \mu\text{g m}^{-3}$ that was generated from the mixture. That the single ROG yields used in conjunction with eq 7 account for the organic aerosol mass concentrations generated in the multiple ROG experiments clearly shows that an absorption model appears to correctly represent SOA formation.

Ambient SOA Yields. Ambient SOA yields cannot be represented by a unique value for a given ROG, because they are dependent on organic aerosol mass concentration and temperature. Examination of eqs 2,3, and 7 suggests that the only differences between the yields obtained from smog chamber studies and those in the ambient environment, for a given M_0 and temperature, will be due to differences in the mean molecular weight of the absorbing om phase and in the activity coefficients of the absorbing products in the om phase. In smog chamber studies, the om phase is generated from the products of oxidation of a single ROG; in the ambient environment, the om phase is comprised of a mixture of condensed primary and secondary species. Even though there will be differences in the mean molecular weight of the om phase and in the activity coefficients between smog chamber SOA and ambient atmospheric aerosol, it seems unlikely that these differences will be large.

The mean molecular weight of the om phase is most likely in the range of $150\text{--}250 \text{ g mol}^{-1}$ both in smog chamber studies and in the ambient environment. On days when SOA formation in the atmosphere is important and oxidation products comprise a significant fraction of the om phase, activity coefficients for SOA products in the ambient om phase will likely be similar to those for SOA products in smog chamber-generated secondary organic aerosol. This hypothesis is supported by the fact that the individual ROG yield data were able to so accurately account for the organic

aerosol mass that was generated in the ROG mixture experiments. For example, if the products of α -pinene and *m*-xylene oxidation had significantly different polarities, then the activity coefficients of the products from *m*-xylene oxidation would be different if those products were partitioned into an organic aerosol layer comprised entirely of *m*-xylene oxidation products as opposed to an organic aerosol layer that was comprised of the oxidation products of both *m*-xylene and α -pinene. This would mean that the yield for *m*-xylene would be different, for a given organic aerosol mass concentration, depending on whether it was measured from an experiment in which only *m*-xylene was used or whether a mixture of *m*-xylene and some other ROG was used. If this were the case, then the organic aerosol mass concentrations in the ROG mixture experiments would not be so accurately accounted for by the individual yield data. This is rather significant because it suggests that SOA yield data obtained from smog chamber studies may likely account for the yield of individual ROG when applied to the ambient atmosphere and could thus be used in conjunction with ambient models to determine the important sources of secondary organic aerosol in an urban airshed.

Acknowledgments

This work was supported by the U.S. Environmental Protection Agency Exploratory Environmental Research Center on Airborne Organics (R-819714-01-0), the National Science Foundation Grant ATM-9307603, the Coordinating Research Council (A-5-1), and the Chevron Corporation.

Literature Cited

- (1) Pankow, J. F. *Atmos. Environ.* **1994**, *28A*, 185–188.
- (2) Pankow, J. F. *Atmos. Environ.* **1994**, *28A*, 189–193.
- (3) Turpin, B. J.; Huntzicker, J. J. *Atmos. Environ.* **1995**, *29B*, 3527–3544.
- (4) Schauer, J. J.; Rogge, W. F.; Hildermann, L. M.; Mazurek, M. A.; Simoneit, B. R.; Cass, G. R. *Atmos. Environ.*, in press.
- (5) Grosjean, D.; Seinfeld, J. H. *Atmos. Environ.* **1989**, *23*, 1733–1747.
- (6) Pandis, S. N.; Harley, R. A.; Cass, G. R.; Seinfeld, J. H. *Atmos. Environ.* **1992**, *26A*, 2269–2282.
- (7) Pandis, S. N.; Wexler, A. S.; Seinfeld, J. H. *Atmos. Environ.* **1993**, *27A*, 2403–2416.
- (8) Pandis, S. N.; Paulson, S. E.; Seinfeld, J. H.; Flagan, R. C. *Atmos. Environ.* **1991**, *25A*, 997–1008.
- (9) Wang, S. C.; Paulson, S. E.; Grosjean, D.; Flagan, R. C.; Seinfeld, J. H. *Atmos. Environ.* **1992**, *26A*, 403–420.
- (10) Hatakeyama, S.; Izumi, K.; Fukuyama, T.; Akimoto, H.; Washida, N. *J. Geophys. Res.* **1991**, *96*, 947–958.
- (11) Izumi, K.; Fukuyama, T. *Atmos. Environ.* **1990**, *24A*, 1433–1441.
- (12) Stern, J. E.; Flagan, R. C.; Grosjean, D.; Seinfeld, J. H. *Environ. Sci. Technol.* **1987**, *21*, 1224–1231.
- (13) Gery, M. W.; Fox, D. L.; Jeffries, H. E. *Int. J. Chem. Kinet.* **1985**, *17*, 931–955.
- (14) Leone, J. A.; Flagan, R. C.; Grosjean, D.; Seinfeld, J. H. *Int. J. Chem. Kinet.* **1985**, *17*, 177–216.
- (15) Grosjean, D. *Aerosols*. In *Ozone and Other Photochemical Oxidants*; National Academy of Sciences: Washington, DC, 1977; Chapter 3, pp 45–125.
- (16) Zhang, S.; Shaw, M.; Seinfeld, J. H.; Flagan, R. C. *J. Geophys. Res.* **1992**, *97*, 20,717–20,729.
- (17) Zhang, S.; Akutsu, Y.; Russell, L. M.; Flagan, R. C.; Seinfeld, J. H. *Aerosol Sci. Technol.* **1995**, *23*, 357–372.
- (18) Atkinson, R. *J. Phys. Chem. Ref. Data* **1989**, *Monograph 1*, 1.
- (19) Atkinson, R.; Aschmann, S. M.; Arey, J. *Int. J. Chem. Kinet.* **1991**, *23*, 77–97.
- (20) Grosjean, D. *Sci. Total Environ.* **1991**, *100*, 367–414.

Received for review December 18, 1995. Revised manuscript received April 17, 1996. Accepted April 19, 1996.*

ES950943+

* Abstract published in *Advance ACS Abstracts*, June 15, 1996.